ADVANCES IN ATMOSPHERIC SCIENCES, VOL. 35, FEBRUARY 2018, 224–233

• **Original Paper** •

Aerosol Properties and Their Impacts on Surface CCN at the ARM Southern Great Plains Site during the 2011 Midlatitude Continental Convective Clouds Experiment

Timothy LOGAN[1], Xiquan DONG*[2], and Baike XI[2]

[1]*Department of Atmospheric Sciences, Texas A&M University, College Station, TX* 77843-3150*, USA*
[2]*Department of Hydrology and Atmospheric Sciences, University of Arizona, Tucson, AZ* 85721-0081*, USA*

(Received 7 February 2017; revised 7 April 2017; accepted 22 May 2017)

ABSTRACT

Aerosol particles are of particular importance because of their impacts on cloud development and precipitation processes over land and ocean. Aerosol properties as well as meteorological observations from the Department of Energy Atmospheric Radiation Measurement (ARM) platform situated in the Southern Great Plains (SGP) are utilized in this study to illustrate the dependence of continental cloud condensation nuclei (CCN) number concentration ($N_{\rm CCN}$) on aerosol type and transport pathways. ARM-SGP observations from the 2011 Midlatitude Continental Convective Clouds Experiment field campaign are presented in this study and compared with our previous work during the 2009–10 Clouds, Aerosol, and Precipitation in the Marine Boundary Layer field campaign over the current ARM Eastern North Atlantic site. Northerly winds over the SGP reflect clean, continental conditions with aerosol scattering coefficient ($\sigma_{\rm sp}$) values less than 20 Mm^{-1} and $N_{\rm CCN}$ values less than 100 cm^{-3}. However, southerly winds over the SGP are responsible for the observed moderate to high correlation (R) among aerosol loading ($\sigma_{\rm sp} > 60$ Mm^{-1}) and $N_{\rm CCN}$, carbonaceous chemical species (biomass burning smoke), and precipitable water vapor. This suggests a common transport mechanism for smoke aerosols and moisture via the Gulf of Mexico, indicating a strong dependence on air mass type. NASA MERRA-2 reanalysis aerosol and chemical data are moderately to highly correlated with surface ARM-SGP data, suggesting that this facility can represent surface aerosol conditions in the SGP, especially during strong aerosol loading events that transport via the Gulf of Mexico. Future long-term investigations will help to understand the seasonal influences of air masses on aerosol, CCN, and cloud properties over land in comparison to over ocean.

Key words: aerosol indirect effect, aerosol transport, biomass burning smoke

Citation: Logan, T., X. Q. Dong, and B. K. Xi, 2018: Aerosol properties and their impacts on surface CCN at the ARM Southern Great Plains site during the 2011 Midlatitude Continental Convective Clouds Experiment. *Adv. Atmos. Sci.*, **35**(2), 224–233, https://doi.org/10.1007/s00376-017-7033-2.

1. Introduction

Aerosol particles exhibit major impacts on cloud development and precipitation processes (Rosenfeld et al., 2008; Li et al., 2011). Though the aerosol direct effect can simply be thought of as a reduction of incoming solar radiation reaching the Earth's surface, the aerosol indirect effect (AIE) involves a complex set of aerosol–cloud–precipitation interactions. These indirect effects include the alteration of cloud microphysical properties such as cloud lifetime, droplet size distribution, liquid water content (LWC), ice water content, liquid water path (LWP), ice water path, cloud optical depth, and albedo (Penner et al., 2004; Dong et al., 2005, 2006, 2014). Precipitation processes will certainly be affected in numerous and, at times, detrimental ways (Wang et al., 2009; Li et al., 2011; Guo et al., 2014). Hence, there is a major impact to society as a whole due to a heavy dependence on the distribution of available water over a given region for public consumption, agriculture, and industrial purposes.

Urban areas are primary sources of sulfate, nitrate, ammonium, and carbonaceous aerosols generated by factory emissions and car exhaust. Numerous studies have shown that the cloud condensation nuclei (CCN) number concentration ($N_{\rm CCN}$) typically increases downwind of urban areas, leading to thicker clouds with longer lifetimes and more precipitation (Rosenfeld et al., 2008; Tao et al., 2012; Leng et al., 2014). Biomass smoke aerosols account for over half of the global carbonaceous aerosol content and are produced primarily from agricultural burning and wildfires (Lyons et al., 1998; Reid and Hobbs, 1998; Wang et al., 2009). These aerosols are being examined for the potential to perturb cloud development and have been studied in the Amazon and Southeast Asia (Reid and Hobbs, 1998; Rosenfeld, 1999;

* Corresponding author: Xiquan DONG
Email: xdong@email.arizona.edu

Graf et al., 2009) due to their constant generation in these regions. Biomass smoke can either enhance or suppress cloud development depending on the chemical nature of the particles (Rosenfeld, 1999; Rosenfeld et al., 2008; Tao et al., 2012). More studies are being conducted in North and Central America due to the possible link between biomass burning smoke and its possible influence on deep convection in the Southern Great Plains (SGP) region of the United States (Wang et al., 2009; Saide et al., 2015). Hence, cloud microphysical properties are sensitive to ambient aerosol particle concentrations; though, admittedly, the science behind this sensitivity is extremely complex (Koren et al., 2005; Rosenfeld et al., 2008; Camponogara et al., 2014; Fan et al., 2015).

The 2011 Midlatitude Continental Convective Clouds Experiment (MC3E) was an intensive field campaign conducted over the SGP region from 22 April to 6 June 2011 (Jensen et al., 2016). The primary goal of MC3E was to study not only deep convective cloud microphysical processes, but also the environment in which these clouds develop over land. A combination of surface, aircraft, and satellite observations was collected during the campaign. The Department of Energy (DOE) Atmospheric Radiation Measurement (ARM) facility, located in north-central Oklahoma, provided continuous surface measurements of variables such as aerosol particle physical and chemical properties and N_{CCN}, in addition to local precipitation amounts, throughout the entire campaign period. The comprehensiveness of the multi-platform observations during MC3E made this campaign an ideal test bed for the observational investigation of aerosol influences on continental cloud development. Thus, the MC3E campaign is a fortuitous opportunity to compare aerosol influences on N_{CCN} over land with our previous study that was conducted over the Eastern North Atlantic Ocean site (Logan et al., 2014).

The primary goals of this companion study are as follows: (1) analyze the physical and chemical nature and origins of the aerosol particles using ARM-SGP surface-based observations and trajectory analysis during MC3E (25 April to 25 May 2011); and (2) elucidate their ability to activate as CCN, as well as their influences on N_{CCN}, with respect to the nature of the air masses that transport them. This study builds upon the methodology of our previous work by adding a chemical component to verify aerosol type, and using other parameters such as precipitable water vapor (PWV) and LWP to show the dependence of cloud development on aerosol (CCN) and air mass type. Section 2 outlines the methodology, instrumentation, and observations used in this study. Section 3 provides an analysis of the aerosol optical and chemical properties, statistical connections with N_{CCN}, identification of the source region of the aerosols during MC3E, and air mass characteristics. Section 4 summarizes the study's key findings and discusses areas of focus for future research.

2. Data and methodology

The ARM-SGP central facility (36.6°N, 97.5°W) employs surface-based instruments and remote sensing equipment that can provide continuous measurements of the physical and chemical properties of atmospheric constituents, such as gases, aerosols, and clouds, as well as local meteorological conditions (e.g., wind, temperature, precipitation, and atmospheric profiles). The facility is located in a region of the United States where it can sample air from surrounding areas and neighboring states, as well as aerosols that advect from the Gulf of Mexico and Central America (Fig. 1). The ARM Aerosol Observation System (AOS) has several surface-based (10 m above ground-level) instruments that can retrieve physical and chemical information of aerosol particles at the lowest levels of the atmosphere. The AOS platform features a nephelometer (Model 3563, TSI, http://www.tsi.com/), a cloud condensation nuclei counter (Droplet Measurement Technologies, http://www.dropletmeasurement.com/), and an Aerodyne Aerosol Chemical Speciation Monitor (ACSM, http://www.aerodyne.com/).

The nephelometer can measure the aerosol scattering coefficient (σ_{sp}) at three wavelengths (450, 550, and 700 nm). This instrument uses a filter that captures and analyzes aerosol particles with aerodynamic diameters (i.e., irregularly shaped particles possessing the same settling velocity of spherical particles of equal size), D_p, of 10 μm and lower at 40% relative humidity to minimize any hygroscopic effects (Jefferson, 2011). The data are measured at a 1-minute temporal resolution and have been geometrically corrected (Anderson and Ogren, 1998). The total aerosol scattering coefficient at the green wavelength ($\sigma_{sp,550}$) of particles ($D_p \leqslant 10$ μm) is used to denote aerosol loading and is analogous to similar retrievals of aerosol optical depth (AOD) at the mid-visible wavelength (Logan et al., 2014). In general, background continental aerosol loading is typically less than 10 Mm^{-1}, but can be higher depending on the proximity to aerosol source regions, such as urban/industrial centers or agriculture (Bergin, 2000; Logan et al., 2014). Therefore, this study denotes $\sigma_{sp,550}$ less than 20 Mm^{-1} as background or "clean" conditions, and strong aerosol loading as having values that exceed 60 Mm^{-1} (three times the background) (Bergin, 2000; Logan et al., 2014).

The single-column Data Management Team Model 1 cloud condensation nuclei counter uses an optical particle counter that measures the surface aerosols that are able to activate as CCN at seven supersaturation levels (Jefferson, 2011; Uin, 2016). The data have a temporal resolution of 1 h because the CCN counter normally needs roughly 5–10 min to stabilize and measure N_{CCN} at each supersaturation level. This study uses the 0.2% supersaturation level to represent atmospheric conditions of moderate to strong aerosol loading in the presence of low-level clouds (Hudson and Noble, 2014; Leng et al., 2014; Liu and Li, 2014; Logan et al., 2014).

The ACSM employs a thermal vaporization, electron impact ionization mass spectrometer that can measure ground-level species, such as carbonaceous compounds (black and organic carbon) and ions of sulfate, nitrate, ammonium, and chloride, with a 30-min temporal resolution in units of μg m^{-3} (Ng et al., 2011). Chemical species such as sulfate, ni-

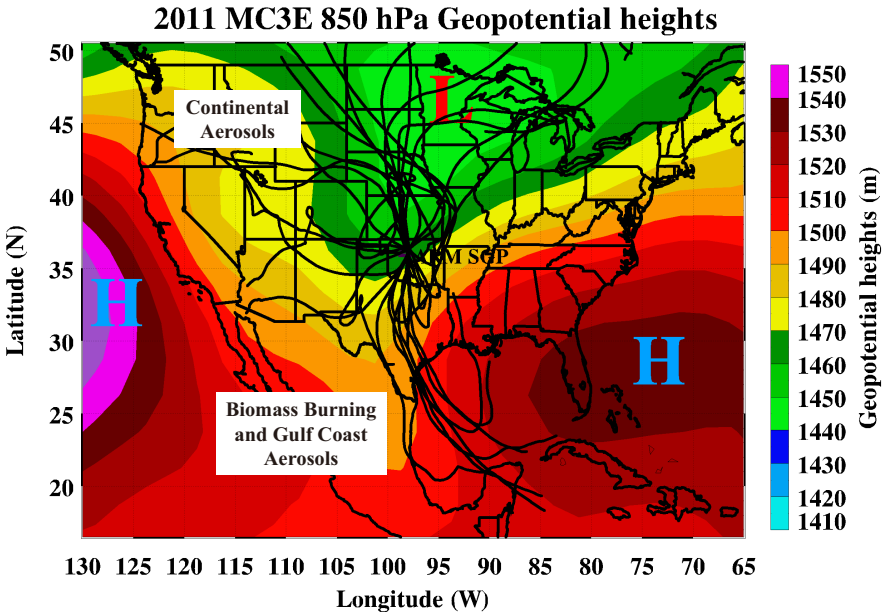

Fig. 1. Aerosol transport pathways over the ARM-SGP site as given by the mean 850 hPa heights (boundary layer) and backward trajectories over the entire MC3E campaign (25 April to 25 May 2011). Note the average positions of the trough (cyclonic rotation) and two ridges (anticyclonic rotation) are conducive to aerosol and moisture transport from the south (Mexico and the Gulf Region) and continental aerosol transport from the north and west.

trate, and ammonium ions can denote anthropogenic aerosols derived from pollution and agriculture (Hudson et al., 2004; Ng et al., 2011; Liu and Li, 2014). Black and organic carbon compounds are the main combustion products of biomass materials (e.g., trees and vegetation). Therefore, the carbonaceous species concentration is used to denote aerosol particles derived from biomass burning smoke (Ng et al., 2011). Note that, though the ACSM alone is not sufficient to determine aerosol type, it is used in conjunction with the other measurement platforms, trajectory analysis, meteorological observations, and reanalysis data to verify the location and movement of the air masses over aerosol source regions.

3. Results and discussion

In this section, we present the trajectory analysis, aerosol, cloud, and moisture environment during MC3E. Furthermore, we discuss the conditions in which aerosol particles can influence N_{CCN} through an integrative analysis of ground-based ARM-SGP observations and retrievals. Simulations of AOD and black carbon (BC) data from the second NASA Modern Era Retrospective Reanalysis for Research (MERRA-2) model are used in this study to provide more spatial coverage and lend support to the ARM-SGP measurements during MC3E. Note that this study assumes that aerosol particles originating from the near surface (e.g., within the boundary layer) serve as the CCN responsible for cloud development (Logan et al., 2014).

3.1. *Dynamics and trajectory analysis*

During the spring months (March, April and May) of 2011, there were numerous episodes of biomass burning smoke being transported via the Gulf of Mexico to the SGP region. Synoptic and mesoscale dynamics play important roles in governing the movement of the air masses that transport aerosols from their source to sink regions (Logan et al., 2010, 2014; Tao et al., 2013). Figure 1 shows the NOAA/ESRL reanalysis mean 850 hPa geopotential heights (Kalnay et al., 1996) along with the mean positions of two upper-level high pressure systems (ridges) and an upper-level low pressure system (trough) during the MC3E campaign. A ridge centered over the Atlantic Ocean is responsible for the southerly transport of Gulf of Mexico moisture and aerosols from Mexico and Central America. Continental aerosols are transported from the combination of a ridge centered over the eastern Pacific Ocean and a trough centered near the Great Lakes region. The NOAA Hybrid Single-Particle Lagrangian Integrated Trajectory (HYSPLIT) (Rolph, 2012; Draxler and Rolph, 2013; Stein et al., 2015) model computes the backward trajectories of parcels within the air masses (Leng et al., 2014). The model is initialized at 1800 UTC and is run each day from 25 April to 25 May 2011 using a height of 500 m (represents near-surface or sub-cloud, boundary layer air). There is a clear distinction between the southerly and northerly trajectories denoting the direction of air transport to the SGP region via continental and marine air masses (Fig. 1).

As illustrated in Fig. 2, the trajectories are partitioned by N_{CCN} magnitude, which range from clean ($N_{CCN} < 500$ cm^{-3}) to strongly polluted ($N_{CCN} > 1500$ cm^{-3}) conditions. AOD retrievals from the Moderate Resolution Imaging Spectroradiometer onboard the Terra satellite (MODIS-Terra) Combined Deep Blue/Dark Target product (e.g., NASA Giovanni) are used to show not only the general aerosol loading during

the entire MC3E campaign, but also hotspots of aerosol activity. The cleaner trajectories are primarily from regions north of the ARM-SGP site. This reflects source regions of continental air that are generally devoid of active fires (fire data provided by satellite at http://earthdata.nasa.gov/data/near-real-time-data/data/hazards-and-disasters/fires). Note that there are few densely populated areas and no megacities along the paths of the clean trajectories. The weakly and moderately polluted trajectories ($N_{CCN} \sim 500$–1500 cm^{-3}) have origins both south and north of the ARM-SGP site and denote air parcels that likely contain aerosols from satellite-confirmed fires in the midwestern and southwestern regions of the United States (Figs. 2b and c). The strongly polluted trajectories are mainly observed as coming from the south via the Gulf of Mexico (Fig. 2d). Figure 3 illustrates the origins of air masses containing carbonaceous (BC) aerosols. Though the trajectories with the highest BC content come primarily from the south, there are instances of weakly and moderately polluted trajectories originating from the west. During the period of the MC3E campaign, there were confirmed incidences of wildfires and dust events in areas west of the ARM-SGP site. For example, there are instances of elevated mean AOD (~ 0.2) in the Texas panhandle, northeastern New Mexico, eastern Colorado, and western Arizona.

As previously discussed, biomass burning smoke has been observed during the spring season over the Gulf of Mexico for decades and is mainly attributed to agricultural burns and wildfires in Mexico and Central America (Peppler et al., 2000; Wang et al., 2009). In addition, the Gulf Coast has numerous urban/industrial areas that include the megacity of Houston, Texas, along with petrochemical facilities and shipping lanes generating pollution throughout the year. The pollution and smoke aerosols tend to be confined closer to the surface during humid, stagnant conditions, while long-range transported aerosols, in general, are able to reach the surface via subsidence, entrainment, and turbulent processes between the interface of the free troposphere and boundary layer (Leng et al., 2014; Logan et al., 2014; Dong et al., 2015).

3.2. *Physical and chemical properties of aerosol particles and N_{CCN} during MC3E*

Figure 4a shows the time series of $\sigma_{sp,550}$, N_{CCN}, and CCN activation rates given by the ratio of condensation nuclei number concentration (N_{CN}) to N_{CCN} from 0000 UTC 25 April to 0000 UTC 25 May 2011. In general, N_{CCN} increases (decreases) with increasing (decreasing) $\sigma_{sp,550}$, with a strong correlation (R-value) of 0.8, suggesting that the surface aerosol particles easily activate as CCN. In fact, when $\sigma_{sp,550}$ exceeds 60 Mm^{-1}, the N_{CCN} exceeds 1000 cm^{-3}. The highest N_{CCN} value (~ 2000 cm^{-3}) corresponds to the highest $\sigma_{sp,550}$ value (~ 100 Mm^{-1}) on 11 May 2011, while the lowest values occur during the period 12–17 May 2011 ($\sigma_{sp} \leqslant 20$ Mm^{-1}, $N_{CCN} \leqslant 500$ cm^{-3}). The sharp decrease in N_{CCN} and σ_{sp} is indicative of a mesoscale precipitation event occurring on 11 May 2011 that removed aerosols via wet deposition (Wang et al., 2016).

The daily-averaged N_{CCN}/N_{CN} ratio values show similar variations, with increases corresponding to periods of strong aerosol loading and decreases corresponding to cleaner conditions. The lowest ratios denote continental aerosols that do not activate efficiently as CCN, such as mineral dust observed over the SGP region by satellite (not shown) on 12–14 May 2011. After the passage of a strong cold front on 11 May 2011, westerly winds transported dust from New Mexico and the Texas panhandle into the region. In this instance, the dust aerosols do not activate well as CCN given the drier conditions after the frontal passage (Logan et al., 2014). Moreover, all ratios that are less than 10% correspond to trajectories that are north and west of the ARM-SGP site (Fig. 2 and Fig. 3), further denoting continental air. The highest ratios are observed during polluted conditions as a result of smoke being transported from the south, as shown by the trajectories in Fig. 2 and Fig. 3. The ratios approach 60% on May 11, which suggests the majority of smoke aerosols do activate as CCN. However, it is important to note that aging, hygroscopicity (or "kappa"), and the overall chemical nature of the smoke particles can impact the activation rate and subsequent contribution to overall aerosol loading (Petters and Kreidenweis, 2007). In fact, long-term future investigations will attempt to quantify this behavior using more observation and modeling data.

Figure 4b shows the surface aerosol chemical properties from the AOS measurements where the carbonaceous concentration is dominant with an order of magnitude higher than those from sulfate, ammonium, and nitrate. The maxima of the chemical species concentrations and N_{CCN} are also strongly correlated ($R \sim 0.84$). This suggests that both smoke and pollution aerosols influence the aerosol particle chemistry, with smoke being the largest contributor (Lyons et al., 1998; Kreidenweis et al., 2001; Hudson et al., 2004; Koren et al., 2005). Note that the smoke aerosols are not initially hygroscopic, but can undergo aging during transport and oxidize to a more water-soluble form, and therefore readily activate as CCN, as demonstrated in the conceptual model depicted in Fig. 5.

PWV is the vertically integrated amount of water vapor in an atmospheric column, while the LWP is the total amount of column liquid water (Liljegren et al., 2001). PWV describes the maximum amount of precipitation observed if all moisture in a given area could condense, while LWP is more related to cloud properties such as droplet size, optical depth, and cloud LWC (Dong et al., 2000). Figure 4c shows examples of collocated peaks of PWV (> 30 mm) and LWP (> 1000 g m^{-2}), which denote precipitation events and a subsequent change in air mass (wind direction) from polluted (southerly wind) to clean (northerly wind). This is synonymous with a change in moisture conditions from marine (humid) to continental (dry), which is supported by the trajectory analysis (Fig. 2). The overall trend in PWV is similar to the aerosol loading, N_{CCN} and chemical species, with a moderate correlation ($R \sim 0.5$), suggesting that the water vapor and aerosols are likely in-phase and aligned along the same transport pathway. The observed trends in σ_{sp}, N_{CCN},

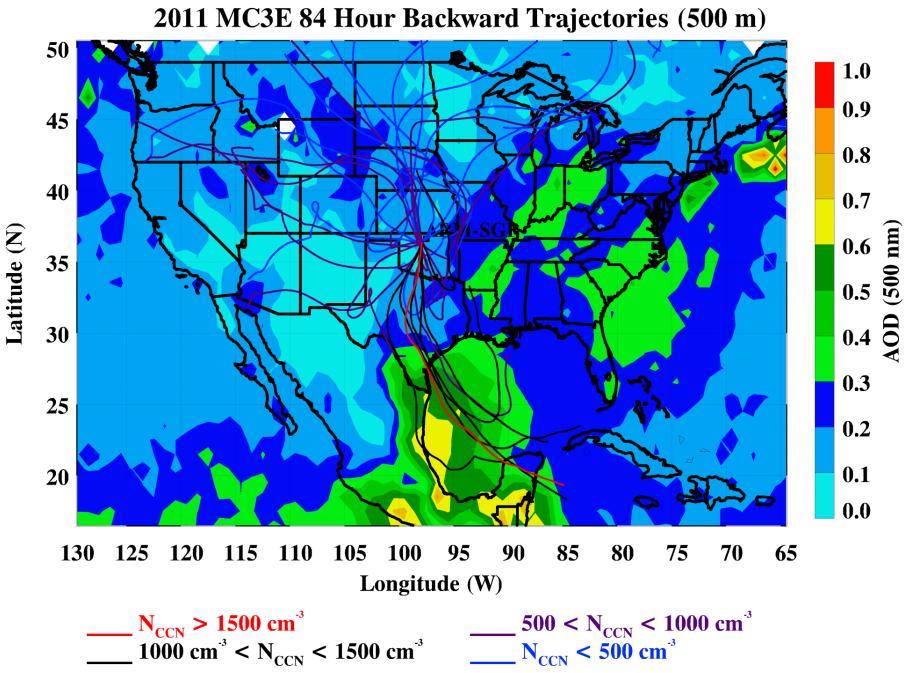

Fig. 2. MODIS-Terra AOD with HYSPLIT sub-cloud backward trajectories during MC3E. 30-day area-averaged AOD values are used with trajectories denoting clean (blue lines), weakly polluted (purple lines), moderately polluted (black lines), and strongly polluted (red lines) air parcels. Note the trajectories that pass over the Gulf Coast and Gulf of Mexico (to the south) are typically more polluted than trajectories that pass over land (from the north and west).

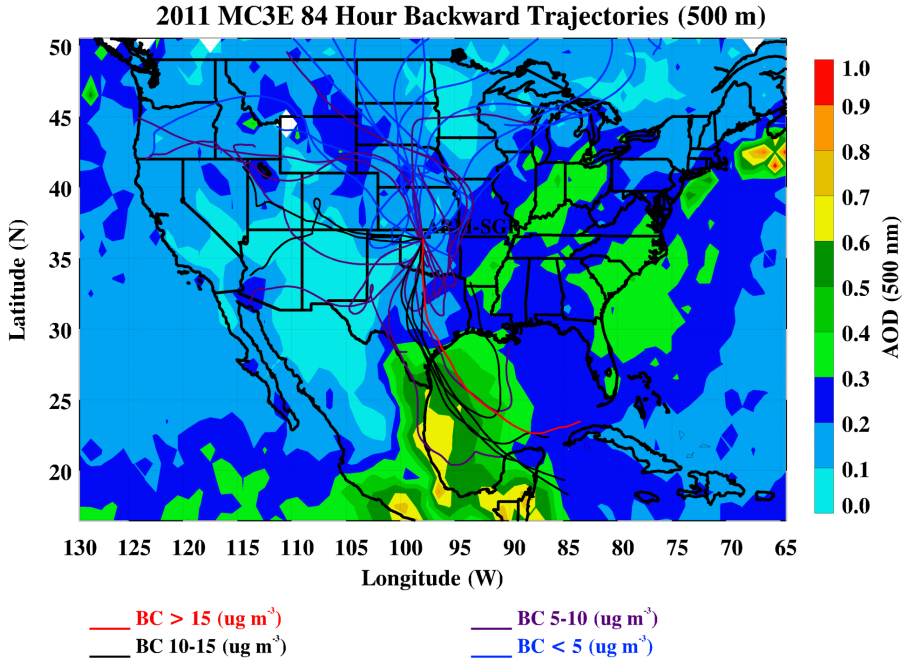

Fig. 3. As in Fig. 2 but for carbonaceous aerosols (BC). Note that, similar to Fig. 2, air masses originating from the north contain less BC than air masses originating from the north. Trajectories that are weakly and moderately polluted that originate from the west are indicative of biomass burning smoke from confirmed wildfires within the United States.

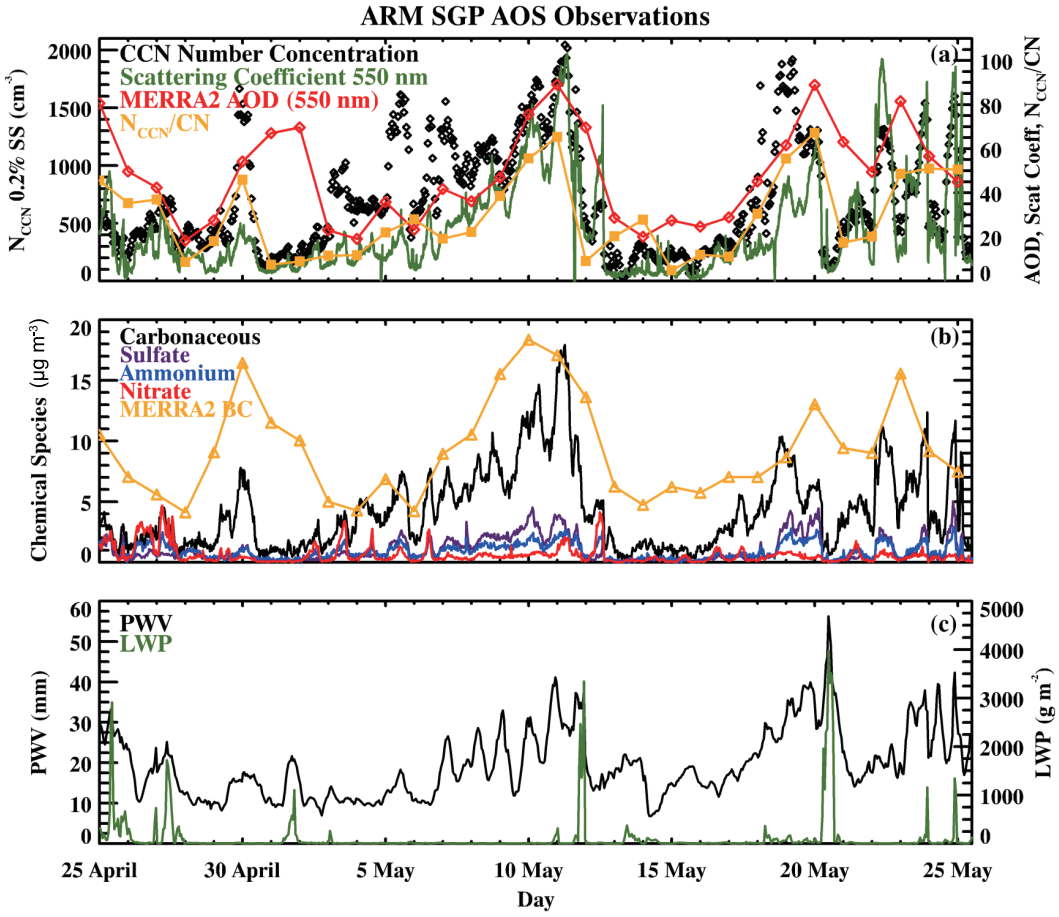

Fig. 4. ARM-SGP surface observations and sub-cloud backward trajectory analysis during MC3E: (a) N_{CCN} at 0.2% supersaturation (black diamonds) along with the aerosol scattering coefficient (σ_{sp}) at the 550 nm wavelength in units of Mm^{-1} (green solid line), MERRA-2 AOD data (red-diamond line with values multiplied by 175 for fit), and daily-averaged aerosol-to-CCN activation ratios (gold-box line with values multiplied by 100 for fit) on the secondary *y*-axis; (b) carbonaceous (black solid line) and inorganic chemical constituents (purple, blue, and red solid lines) of the surface aerosols (sulfate, ammonium, and nitrate, respectively) along with MERRA-2 BC data in units of kg m^{-2} (gold-triangle line multiplied by 60 000 for fit); (c) PWV and cloud LWP retrieved from microwave radiometer brightness measurements (black and green solid lines, respectively).

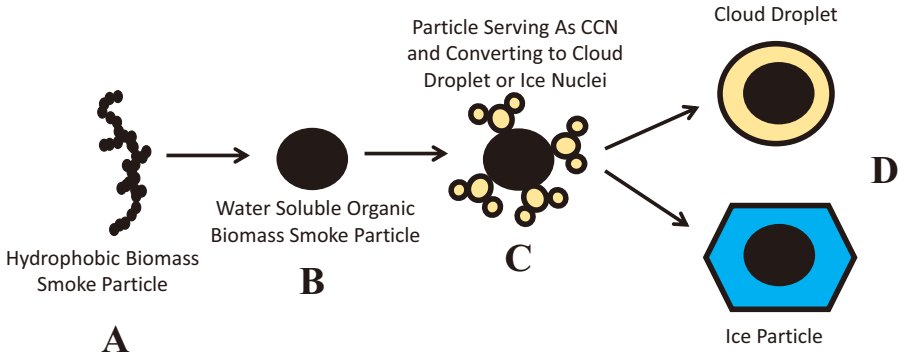

Fig. 5. Conceptual model of a biomass burning smoke particle becoming a cloud droplet (A–C). The hydrophobic smoke particle (A) are aged and oxidized by sunlight and/or gas-phase radicals to a more water-soluble form (B) and becomes a CCN. Net condensation (hygroscopic growth) occurs around the smoke particle (C) to create cloud droplets or ice particles (D) depending on the updraft strength in the cloud (i.e., strong updrafts can lift CCN above the freezing level).

and PWV during MC3E further illustrate the shared transport pathway of Gulf moisture, pollution, and biomass burning smoke, which stresses the importance of conducting a long-term research effort that investigates the sensitivity of clouds and precipitation processes to changes in air mass type.

3.3. *MERRA-2 simulations of AOD and BC*

MERRA-2 offers a large improvement over the previous generation of MERRA model data products. MERRA-2 uses an updated version of the NASA Goddard Earth Observing System atmospheric data assimilation system, which is capable of incorporating newer types of satellite data (e.g., Aura, MODIS, Suomi NPP, GOES) (Buchard et al., 2015; McCarty et al., 2015). The data have a spatial coverage of $0.5^\circ \times 0.625^\circ$ and are output either hourly or monthly, with the former being used in this study. The AOD and BC data products are compared with the ARM-SGP σ_{sp} and carbonaceous content observations during the entire MC3E campaign, along with a heavily polluted episode (5–12 May 2011) over the SGP.

Figures 4a and 4b show the temporal variations in AOD and BC assimilated by MERRA-2 during MC3E. Compared to the ARM-SGP observations, there are similarities between the MERRA-2 simulations and ARM-SGP observations; notably, sharp increases in aerosols during 30 April to 1 May 2011, a gradual increase during 5–11 May 2011, and peaks at 20 May and 23 May 2011. Recall that the largest aerosol loading occurred on 11 May 2011. Though the trends in MERRA-2 are not perfectly in-phase with the ARM-SGP results, the model does an adequate job of capturing the same timeframe and magnitude of the aerosol episodes as the surface-based instruments.

The correlations between MERRA-2 and ARM-SGP AOD and BC data are shown in Tables 1 and 2, respectively. In addition, correlations with PWV (moisture content) are also provided. Two scenarios are presented: correlations for the entire month, and a selected pollution event (5–11 May 2011). MERRA-2 AOD has an overall weaker correlation with ARM-SGP σ_{sp} and N_{CCN} during MC3E ($R < 0.6$). This is likely due to a combination of uncertainties associated with comparing column to point measurements and the assumption that all aerosols can act as CCN, especially at the surface. In addition, Buchard et al. (2015) pointed out that the satellite retrieval algorithms used by MERRA-2 suffer from uncertainties in the presence of clouds and have large differences over land and ocean. However, during the pollution episode, where the aerosols and moisture were aligned along the same transport pathway, there are higher correlations between the two datasets ($R > 0.7$). This suggests that the smoke aerosols that dominated the aerosol content do convert to CCN efficiently, especially over the SGP region. Note that, even during the pollution event, the MERRA-2 AOD correlation only increases from 0.31 to 0.5, which again is due to uncertainties in just how efficient the aerosol activation to CCN process is captured in the model, and therefore warrants further study (e.g., long-term study of the AIE) (Buchard et al., 2015). Two additional causes of uncertainty, (1) representation error between the MERRA-2 (column measurement) and surface AOS (point source) datasets and (2) hygroscopic particle swelling that can lead to increases in total AOD, will also be addressed in future long-term studies.

There are similar findings when taking into account the MERRA-2 BC product, in that higher correlations are observed with ARM-SGP carbonaceous species measurements during the pollution episode ($R > 0.8$). This suggests that there are probably multiple source regions for the smoke aerosols, especially when the air mass switches from the warm and moist Gulf of Mexico air to drier, continental air that may contain smoke from remnant fires west of the

Table 1. Comparison between MERRA-2 AOD and ARM-SGP using aerosol parameters (AOD, σ_{sp}, N_{CCN}, and carbonaceous content) and PWV (moisture parameter).

(a) Correlation during MC3E (25 April to 25 May 2011)

	N_{CCN}	Smoke	Scattering coefficient	MERRA-2 AOD
N_{CCN}	–	–	–	–
Smoke	0.82	–	–	–
Scattering coefficient	0.69	0.82	–	–
MERRA-2 AOD	0.31	0.38	0.56	–
PWV	0.56	0.47	0.67	0.68

(b) Correlation during major pollution episode (2–11 May 2011)

	N_{CCN}	Smoke	Scattering coefficient	MERRA-2 AOD
N_{CCN}	–	–	–	–
Smoke	0.78	–	–	–
Scattering coefficient	0.69	0.97	–	–
MERRA-2 AOD	0.5	0.71	0.83	–
PWV	0.74	0.94	0.97	0.83

Table 2. Comparison between MERRA-2 BC and ARM-SGP using aerosol parameters (AOD, σ_{sp}, N_{CCN}, and carbonaceous content) and PWV (moisture parameter).

(a) Correlation during MC3E (25 April to 25 May 2011)

	N_{CCN}	Smoke	Scattering coefficient	MERRA-2 Smoke
N_{CCN}	–	–	–	–
Smoke	0.82	–	–	–
Scattering coefficient	0.69	0.82	–	–
MERRA-2 Smoke	0.48	0.69	0.66	–
PWV	0.56	0.47	0.67	0.53

(b) Correlation during major pollution episode (2–11 May 2011)

	N_{CCN}	Smoke	Scattering coefficient	MERRA-2 Smoke
N_{CCN}	–	–	–	–
Smoke	0.78	–	–	–
Scattering coefficient	0.69	0.97	–	–
MERRA-2 Smoke	0.5	0.82	0.92	–
PWV	0.74	0.94	0.97	0.89

ARM-SGP site. Though the MERRA-2 data product can show a larger picture of the aerosol burden over the SGP, surface-based ARM-SGP observations do show relatively good agreement with the satellite-ingested data assimilation methods used by MERRA-2.

3.4. *Continental boundary layer and marine boundary layer N_{CCN}*

Since it is assumed that boundary layer CCN are the primary agents in cloud development, how do aerosols that activate as CCN over land compare to those over the ocean? Previous work suggests that wind-driven sea salt is the dominant contributor to aerosol content over the ocean and can regularly activate as CCN, thus contributing to cloud formation (Logan et al., 2014; Dong et al., 2015; Wood et al., 2015). Sulfate aerosols and aged biomass burning smoke also make excellent CCN, while mineral dust activates poorly as CCN, though none of these aerosol types was consistently observed over the Azores region in the study by Logan et al. (2014); specifically, there were only seven cases of moderate aerosol loading ($\sigma_{sp} > 30$ Mm^{-1}) over 19 months.

Over land, the present study shows that biomass burning smoke is an excellent source of continental boundary layer CCN, and has similar episodic intrusions. A future goal of this line of study is to compare and contrast long-term cloud development over land and ocean as a function of the AIE in both regions using surface-based, satellite-retrieved and reanalysis data products of aerosol, cloud, and precipitation properties. In addition, model simulations will also be performed to see which aerosol types have the greatest impacts on precipitation processes.

4. Summary and conclusions

Aerosols and their ability to activate as CCN are investigated over land using observations from the 2011 MC3E campaign conducted over the SGP region of the United States. Trajectory analysis shows that many of the aerosols responsible for increases in N_{CCN} have source regions in Mexico, Central America, and along the Gulf Coast. Further analysis suggests these aerosols consist mainly of biomass burning smoke particles that have been found to easily activate as CCN in a previous study (e.g., Logan et al., 2014). We present the following conclusions:

(1) There are moderate to high correlations ($R > 0.5$) between aerosol loading (σ_{sp}), N_{CCN}, carbonaceous chemical species, and PWV, suggesting a shared common transport pathway via the Gulf of Mexico and further indicating the dependence on moist, tropical marine air masses for transport. However, N_{CCN} values were lowest when a clean, continental air mass was in place over the SGP, except for instances of active wildfires within the region of influence of the air mass.

(2) When comparing ARM-SGP surface observations with the larger spatial coverage MERRA-2 reanalysis data, there is good agreement between the two platforms, suggesting that the ARM-SGP site can serve as a suitable, representative measurement platform, especially during periods of heavy aerosol loading episodes during the spring months when biomass smoke is almost always present over the Gulf of Mexico and transported to the SGP region of the United States. This could aid future investigations looking into the AIE in terms of cloud development over land.

(3) As compared with our previous study, Logan et al. (2014), it is evident that there are some similarities and differences between how aerosols impact N_{CCN} over ocean and land. Both regions see increases in N_{CCN} when biomass burning smoke is the dominant aerosol type but is only observed periodically. In contrast, during clean conditions over the ocean, sea salt is the main contributor to CCN production, and strong (weak) surface winds and turbulent conditions can enhance (diminish) N_{CCN} production (Dong et al., 2015). Over land, there is a strong dependence of N_{CCN} on changes in air mass type from marine to continental (Leng et al., 2014). Further research involving the AIE will focus on examining, over the long-term, how air masses influence cloud properties and precipitation processes over land and ocean.

Acknowledgements. The surface aerosol data were obtained from the ARM Program sponsored by the U.S. DOE Office of Energy Research, Office of Health and Environmental Research, and Environmental Sciences Division. The meteorological data for Figs. 1–3 were obtained from the NOAA ESRL Physical Sciences Division in Boulder, Colorado (http://www.esrl.noaa.gov/psd/). The authors wish to thank the scientists at the DOE ARM-SGP site for maintaining the data used in this study. Analyses and visualizations used in this paper were produced with the NASA Giovanni online data system, developed and maintained by the NASA GES DISC (found at http://giovanni.gsfc.nasa.gov/giovanni/). The authors deeply appreciate the comments and suggestions from the anonymous reviewers of this manuscript. This research was supported by National Science Foundation Collaborative Research under the award number AGS-1700728 at the University of Arizona and AGS-1700796 at Texas A&M University.

REFERENCES

Anderson, T. L., and J. A. Ogren, 1998: Determining aerosol radiative properties using the TSI 3563 integrating nephelometer. *Aerosol Science and Technology*, **29**, 57–69, https://doi.org/10.1080/02786829808965551.

Bergin, M. H., 2000: Aerosol radiative properties and their impacts. *From Weather Forecasting to Exploring the Solar System*, C. Boutron, Ed., EDP Sciences, 51–65.

Buchard, V., and Coauthors, 2015: Using the OMI aerosol index and absorption aerosol optical depth to evaluate the NASA MERRA Aerosol Reanalysis. *Atmos. Chem. Phys.*, **15**, 5743–5760, https://doi.org/10.5194/acp-15-5743-2015.

Camponogara, G., M. A. F. Silva Dias, and G. G. Carrió, 2014: Relationship between Amazon biomass burning aerosols and rainfall over the La Plata Basin. *Atmos. Chem. Phys.*, **14**, 4397–4407, https://doi.org/10.5194/acp-14-4397-2014.

Dong, X. Q., P. Minnis, T. P. Ackerman, E. E. Clothiaux, G. G. Mace, C. N. Long, and J. C. Liljegren, 2000: A 25-month

database of stratus cloud properties generated from ground-based measurements at the Atmospheric Radiation Measurement Southern Great Plains Site. *J. Geophys. Res*., **105**, 4529–4537, https://doi.org/10.1029/1999JD901159.

Dong, X. Q., P. Minnis, and B. K. Xi, 2005: A climatology of midlatitude continental clouds from the ARM SGP central facility: Part I: Low-level cloud macrophysical, microphysical, and radiative properties. *J. Climate*, **18**, 1391–1410, https://doi.org/10.1175/JCLI3342.1.

Dong, X. Q., B. K. Xi, and P. Minnis, 2006: A climatology of midlatitude continental clouds from the ARM SGP central facility. Part II: Cloud fraction and surface radiative forcing. *J. Climate*, **19**, 1765–1783, https://doi.org/10.1175/JCLI3710.1.

Dong, X. Q., B. K. Xi, A. Kennedy, P. Minnis, and R. Wood, 2014: A 19-month record of marine aerosol-cloud-radiation properties derived from DOE ARM mobile facility deployment at the Azores. Part I: Cloud fraction and single-layered MBL cloud properties. *J. Climate*, **27**, 3665–3682, https://doi.org/10.1175/JCLI-D-13-00553.1.

Dong, X. Q., A. C. Schwantes, B. K. Xi, and P. Wu, 2015: Investigation of the marine boundary layer cloud and CCN properties under coupled and decoupled conditions over the Azores. *J. Geophys. Res*., **120**, 6179–6191, https://doi.org/10.1002/2014JD022939.

Draxler, R. R., and G. D. Rolph, 2013: HYSPLIT (HYbrid Single-Particle Lagrangian Integrated Trajectory) Model access via NOAA ARL READY Website. NOAA Air Resources Laboratory, Silver Spring, MD. [Available online from http://ready.arl.noaa.gov/HYSPLIT.php]

Fan, J. W., and Coauthors, 2015: Improving representation of convective transport for scale-aware parameterization: 1. Convection and cloud properties simulated with spectral bin and bulk microphysics. *J. Geophys. Res.*, **120**, 3485–3509, https://doi.org/10.1002/2014JD022142.

Graf, H.-F., J. Yang, and T. M. Wagner, 2009: Aerosol effects on clouds and precipitation during the 1997 smoke episode in Indonesia. *Atmos. Chem. Phys*., **9**, 743–756, https://doi.org/10.5194/acp-9-743-2009.

Guo, X. L., D. H. Fu, X. Guo, and C. M. Zhang, 2014: A case study of aerosol impacts on summer convective clouds and precipitation over northern China. *Atmos. Res*., **142**, 142–157, https://doi.org/10.1016/j.atmosres.2013.10.006.

Hudson, J. G., and S. Noble, 2014: CCN and vertical velocity influences on droplet concentrations and supersaturations in clean and polluted stratus clouds. *J. Atmos. Sci*., **71**, 312–331, https://doi.org/10.1175/JAS-D-13-086.1.

Hudson, P. K., and Coauthors, 2004: Biomass-burning particle measurements: Characteristic composition and chemical processing. *J. Geophys. Res*., **109**, D23S27, https://doi.org/10.1029/2003JD004398.

Jefferson, A., 2011: Aerosol Observing System (AOS) handbook. Tech. Rep. DOE/SC-ARM/TR-014, U.S. Department of Energy, Washington, D. C.

Jensen, M. P., and Coauthors, 2016: The midlatitude continental convective clouds experiment (MC3E). *Bull. Amer. Meteor. Soc*., **97**, 1667–1686, https://doi.org/10.1175/BAMS-D-14-00228.1.

Kalnay, E., and Coauthors, 1996: The NCEP/NCAR 40-year reanalysis project. *Bull. Amer. Meteor. Soc*., **77**, 437–471, https://doi.org/10.1175/1520-0477(1996)077<0437:TNYRP>2.0.CO;2.

Koren, I., Y. J. Kaufman, D. Rosenfeld, L. A. Remer, and Y. Rudich, 2005: Aerosol invigoration and restructuring of Atlantic convective clouds. *Geophys. Res. Lett*., **32**, L14828, https://doi.org/10.1029/2005GL023187.

Kreidenweis, S. M., L. A. Remer, R. Bruintjes, and O. Dubovik, 2001: Smoke aerosol from biomass burning in Mexico: Hygroscopic smoke optical model. *J. Geophys. Res*., **106**, 4831–4844, https://doi.org/10.1029/2000JD900488.

Leng, C., and Coauthors, 2014: Variations of cloud condensation nuclei (CCN) and aerosol activity during fog–haze episode: A case study from Shanghai. *Atmos. Chem. Phys*., **14**, 12 499–12 512, https://doi.org/10.5194/acp-14-12499-2014.

Li, Z. Q., F. Niu, J. W. Fan, Y. G. Liu, D. Rosenfeld, and Y. N. Ding, 2011: Long-term impacts of aerosols on the vertical development of clouds and precipitation. *Nat. Geosci*., **4**, 888–894, https://doi.org/10.1038/ngeo1313.

Liljegren, J. C., E. E. Clothiaux, G. G. Mace, S. Kato, and X. Q. Dong, 2001: A new retrieval for cloud liquid water path using a ground-based microwave radiometer and measurements of cloud temperature. *J. Geophys. Res*., **106**, 14 485–14 500, https://doi.org/10.1029/2000JD900817.

Liu, J. J., and Z. Q. Li, 2014: Estimation of cloud condensation nuclei concentration from aerosol optical quantities: Influential factors and uncertainties. *Atmos. Chem. Phys*., **14**, 471–483, https://doi.org/10.5194/acp-14-471-2014.

Logan, T., B. K. Xi, X. Q. Dong, R. Obrecht, Z. Q. Li, and M. Cribb, 2010: A study of Asian dust plumes using satellite, surface, and aircraft measurements during the INTEX-B field experiment. *J. Geophys. Res*., **115**, D00K25, https://doi.org/10.1029/2010JD014134.

Logan, T., B. K. Xi, and X. Q. Dong, 2014: Aerosol properties and their influences on marine boundary layer cloud condensation nuclei at the ARM mobile facility over the Azores. *J. Geophys. Res.*, **119**, 4859–4872, https://doi.org/10.1002/2013JD021288.

Lyons, W. A., T. E. Nelson, E. R. Williams, J. A. Cramer, and T. R. Turner, 1998: Enhanced positive cloud-to-ground lightning in thunderstorms ingesting smoke from fires. *Science*, **282**, 77–80, https://doi.org/10.1126/science.282.5386.77.

McCarty, W., D. Considine, T. Lee, C. Randles, L. Coy, K. Wargan, M. Bosilovich, and R. Gelaro, 2015: Use of Satellite Observations in NASA Reanalyses: MERRA-2 and Future Plans. Tech. Rep. NASA CGMS-43 NASA-WP-06, v1, 1–15.

Ng, N. L., and Coauthors, 2011: An aerosol chemical speciation monitor (ACSM) for routine monitoring of the composition and mass concentrations of ambient aerosol. *Aerosol Science and Technology*, **45**, 780–794, https://doi.org/10.1080/02786826.2011.560211.

Penner, J. E., X. Q. Dong, and Y. Chen, 2004: Observational evidence of a change in radiative forcing due to the indirect aerosol effect. *Nature*, **427**, 231–234, https://doi.org/10.1038/nature02234.

Peppler, R. A., and Coauthors, 2000: ARM southern Great Plains site observations of the smoke pall associated with the 1998 Central American fires. *Bull. Amer. Meteor. Soc*., **81**, 2563–2591, https://doi.org/10.1175/1520-0477(2000)081<2563:ASGPSO>2.3.CO;2.

Petters, M. D., and S. M. Kreidenweis, 2007: A single parameter representation of hygroscopic growth and cloud condensation nucleus activity. *Atmos. Chem. Phys*., **7**, 1961–1971, https://doi.org/10.5194/acp-7-1961-2007.

Reid, J. S., and P. V. Hobbs, 1998: Physical and optical properties of young smoke from individual biomass fires in Brazil. *J.*

Geophys. Res., **103**, 32 013–32 030, https://doi.org/10.1029/98JD00159.

Rolph, G. D., 2012: Real-time Environmental Applications and Display sYstem (READY) Website (Available online from http://ready.arl.noaa. gov). NOAA Air Resources Laboratory, Silver Spring, MD.

Rosenfeld, D., 1999: TRMM observed first direct evidence of smoke from forest fires inhibiting rainfall. *Geophys. Res. Lett*., **26**, 3105–3108, https://doi.org/10.1029/1999GL006066.

Rosenfeld, D., U. Lohmann, G. B. Raga, C. D. O'Dowd, M. Kulmala, S. Fuzzi, A. Reissell, and M. O. Andreae, 2008: Flood or drought: How do aerosols affect precipitation? *Science*, **321**, 1309–1313, https://doi.org/10.1126/science.1160606.

Saide, P. E., and Coauthors, 2015: Central American biomass burning smoke can increase tornado severity in the U.S. *Geophys. Res. Lett*., **42**, 956–965, https://doi.org/10.1002/2014GL062826.

Stein, A. F., R. R. Draxler, G. D. Rolph, B. J. B. Stunder, M. D. Cohen, and F. Ngan, 2015: NOAA's HYSPLIT atmospheric transport and dispersion modeling system. *Bull. Amer. Meteor. Soc*., **96**, 2059–2077, https://doi.org/10.1175/BAMS-D-14-00110.1.

Tao, W.-K., J.-P. Chen, Z. Q. Li, C. E. Wang, and C. D. Zhang, 2012: Impact of aerosols on convective clouds and precipitation. *Rev. Geophys*., **50**, RG2001, https://doi.org/10.1029/2011RG000369.

Tao, W.-K., and Coauthors, 2013: Precipitation intensity and variation during MC3E: A numerical modeling study. *J. Geophys. Res.*, **118**, 7199–7218, https://doi.org/10.1002/jgrd.50410.

Uin, J., 2016: Cloud condensation nuclei particle counter instrument handbook. *DOE/SC-ARM-TR-168*, 1-9.

Wang, J., S. C. van den Heever, and J. S. Reid, 2009: A conceptual model for the link between Central American biomass burning aerosols and severe weather over the south central United States. *Environ. Res. Lett*., **4**, 015003, https://doi.org/10.1088/1748-9326/4/1/015003.

Wang, J. Y., X. Q. Dong, B. K. Xi, and A. J. Heymsfield, 2016: Investigation of liquid cloud microphysical properties of deep convective systems: 1. Parameterization raindrop size distribution and its application for stratiform rain estimation. *J. Geophys. Res.*, **121**, 10 739–10 760, https://doi.org/10.1002/2016JD024941.

Wood, R., and Coauthors, 2015: Clouds, aerosols, and precipitation in the marine boundary layer: An arm mobile facility deployment. *Bull. Amer. Meteor. Soc*., **96**, 419–440, https://doi.org/10.1175/BAMS-D-13-00180.1.